Research Article | Vol. 28, No. 21 / 12 October 2020 / Optics Express 31872
Optics EXPRESS

Optical fiber sensor based on a cholesteric liquid crystal film for mixed VOC sensing

YUNHE YANG,[1] DONG ZHOU,[1] XIUJUAN LIU,[1] YONGJUN LIU,[1,2,5] SHUANGQIANG LIU,[3,6] PEIXIAN MIAO,[4] YANCHAO SHI,[4] AND WEIMIN SUN[1]

[1]*Key Lab of In-fiber Integrated Optics, Ministry Education of China, Harbin Engineering University, Harbin 150001, China*
[2]*State Key Laboratory of Applied Optics, Changchun Institute of Optics, Fine Mechanics and Physics, Chinese Academy of Sciences, Changchun 130033, China*
[3]*School of Physics and Astronomy, Sun Yat-Sen University, Zhuhai, Guangdong 519082, China*
[4]*Science and Technology on Vacuum Technology and Physics Laboratory, Lanzhou Institute of Physics, Lanzhou 730000, China*
[5]*liuyj@hrbeu.edu.cn*
[6]*liushq33@mail.sysu.edu.cn*

Abstract: This paper proposes a novel cholesteric liquid crystal (CLC) film–based dual-probe fiber sensor to monitor volatile organic compound (VOC) gas. The sensor consists of a 2×2 multimode fiber coupler, in which the two output fiber ends are covered by two types of CLC films (CLCF) with different pitches. It can be observed that the reflection peak wavelengths of CLCs shift to the red side as the VOC gas concentration increases. The sensitivities of the two CLCFs are 8.435 nm·L/mmol and 14.867 nm·L/mmol to acetone, 14.586 nm·L/mmol and 29.303 nm·L/mmol to ethanol, respectively. In addition, the dependence of the peak wavelength shift of CLCF on the total concentration of the acetone and ethanol mixed gas at different mixing ratios is measured. The linear relationships between the peak shift of CLCFs, the total mixed gas concentration and acetone/ethanol ratio are calculated using the least-squares method. Therefore, this proposed dual-probe fiber optic sensor can distinguish the concentrations of acetone and ethanol in a mixed gas of acetone and ethanol.

1. Introduction

In general, volatile organic compounds (VOCs) are defined as organic chemical compounds with a boiling point below 250°C. Previous studies have reported that VOCs are the major gaseous pollutants and can cause many symptoms such as headaches, inflammation, fatigue, dizziness and nausea. In addition, VOCs may be carcinogenic [1]. By now, various techniques for monitoring the concentrations of VOCs have been proposed, such as multifunctional nanomaterials [2], Gas Chromatography-Mass Spectrometry (GC-MS) [3] and resistive-based gas sensors [4]. Although analytical chemistry techniques have the advantages of high sensitivity and accuracy in detecting VOC concentrations, they require bulky instruments. Therefore, more compact and lighter sensors are desirable for practical applications. The characteristics of fiber optic sensors can meet these requirements and provide new ideas for the realization of VOC sensors [5,6].

To date, various sensitive materials, such as poly (dimethylsiloxane) [7], liquid crystal polymer network [8], semiconductor metal oxide (α-Fe_2O_3, TiO_2) [9,10], graphene [11], zeolite thin film [12] and carbon quantum dots [13] have been reported for VOC detection. Among them, the semiconductor metal oxide sensor has been commercialized. However, it has a relatively high sensitivity only at high temperature (200-500°C), and the detection resolution can reach the level of ppb. When the temperature drops to room temperature, the sensitivity will decrease, and response time and recovery time will increase. Several researches have reported the sensing

#405627 https://doi.org/10.1364/OE.405627
Journal © 2020 Received 18 Aug 2020; revised 26 Sep 2020; accepted 28 Sep 2020; published 7 Oct 2020

Optics EXPRESS

capabilities of liquid crystals(LCs) in sensor applications. The molecular structure of LC has a special functional group, and the direction of the functional group changes with the formation of particular chemical bonds. Therefore, LCs can be used to sense temperature [14], ion [15] and pH [16] LCs also can be utilized to sense chemical agents due to the advantages of fast response, reversibility and high selectivity to chemical agents.

Cholesteric liquid crystals (CLCs) also called chiral nematic liquid crystals, have been widely used as electro-optic materials in display devices. In addition, as responsive materials, the reflection band of CLCs can be adjusted according to chiral material concentration, temperature and light [17,18] Compared with the nematic phases, the cholesteric phases have a self-organized helical structure, in which CLC molecules are arranged in layers, and the average orientation of the molecules in each succeeding layer is rotated by a small angle. The helical pitch is the distance between the two layers after a total rotation of 360° is achieved [19]. When light propagates along the helical axis, the peak wavelength of the selective reflection is $\lambda_0 = np$, where n is the average refractive index of LC and p is helical pitch of CLC. The reflection wavelength can be tuned by changing the environment-sensitive helical pitch. When the CLC molecule is exposed to VOC, it can be regarded as the host-cavities engulf analyte molecules in an enzyme analogous mechanism. The short-range interactions force between liquid crystal molecules is similar to that between VOC molecule and LC. Therefore, the penetration of gas molecules into the CLC helix will cause the pitch (p) to change, resulting in a change in the reflection wavelength [20]. The shift of the reflection wavelength can be used to detect the VOC concentration [21–23]. Recent evidence indicates that multiple VOC gas sensors based on CLC [24–26], such as CLC film [27,28], Polymer stabilized CLC [29], liquid crystalline mixtures [30], nanosize magnetite-doped CLC [31] and CLC-carbon nanotube hybrid architectures [32], have been developed. They use similar principles to change the helical pitch and detect VOC gases. Reference [27] studied a promising sensor formed by a cholesteric film containing functionalized cholesterol derivatives, in which amine vapors can be detected by directly observing the film color. In Ref. [29], colorimetric polymer-stabilized CLC arrays were adopted to monitor amine vapors by examining the reflection spectrum. However, these two methods can only analyze gas qualitatively, not quantitatively. The optical response of an LC composition to VOC gas was investigated in Ref. [30], in which the contrast of CLC decreases when it is exposed to VOC gas. However, due to its high sensitivity to disturbance, this method is unstable and unsuitable for any practical application. References [31] and [32] enhance the response of the helical pitch to external stimuli by doping other substances in CLC. However, the procedures of preparing mixtures are complicated. In addition, these methods can only identify one VOC gas at one time. In order to stably and quantitatively monitor multiple VOC gases at the same time, we propose a dual-probe fiber optic sensor based on CLC membrane.

In this paper, a VOC sensor is fabricated by coating two photopolymerizable CLC films (CLCF) on the output end faces of a 2×2 multimode fiber coupler. As the concentrations of acetone gas and ethanol gas increase, the peak shifts of the reflection wavelengths are observed, respectively. The dependence of the on the total concentration of the acetone and ethanol mixed gas at different mixing ratios is also measured. The concentrations of acetone and ethanol can be detected in a mixed gas of acetone and ethanol using this proposed double-probe fiber optic sensor.

2. Materials and methods

2.1. Materials

The cholesteryl derivatives used in this study are cholesteryl chloride, cholesterol oleyl carbonate, cholesteryl chloroformate, RM257 and photoinitiator. All medicines were purchased from Beijing InnoChem Science&Technology Co., Ltd. The first type of CLC (No.1) is prepared by mixing cholesteryl chloride-12.3 wt%, cholesterol oleyl carbonate-64.4 wt%, cholesteryl

Optics EXPRESS

chloroformate-21.3 wt%, RM257-5 wt% and photoinitiator(2-Benzyl-2-(dimethylamino)-4'-morpholinobutyrophenone)-0.5 wt%, and the second type of CLC (No.2) is produced by mixing cholesteryl chloride-19.8 wt%, cholesterol oleyl carbonate-58.9 wt%, cholesteryl chloroformate-19.3 wt%, RM257-5 wt% and photoinitiator-0.5 wt%. The two mixtures are first heated to 120°C, then sonicated at 80 °C for 30 minutes, and finally naturally cooled to room temperature (25°C).

2.2. Methods

The manufacturing process of the fiber optic probe is shown in Fig. 1(c). We first remove the fiber buffer coating from two fiber ends of a 2 × 2 multimode fiber (MMF) coupler. Next, we cut them flat with a fiber cutter, and then coated the CLC on the end face of the optical fiber through a capillary with an inner diameter of 30 µm, and irradiated with a 20 mW ultraviolet (UV) lamp (Shanghai Luyor Instrument co, Ltd) for 2 mins. The end surface of the fibers will then be covered with a layer of CLCF.

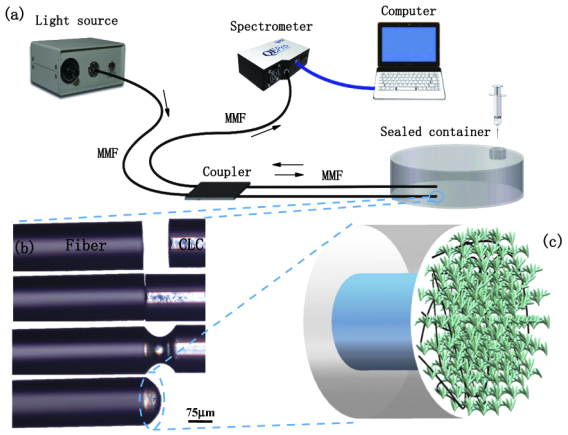

Fig. 1. (a) Schematic diagram of the experimental device; (b) the fabrication process of the fiber-optic probe (polarized light); (c) three-dimensional schematic of the fiber end face.

3. Experimental results and discussion

3.1. Experimental setup and method

Figure 1(a) is the schematic diagram of the experimental device. The white light launched from a tungsten halogen lamp is coupled into an input port of the fiber coupler, and the ends of the CLC-coated output ports are enclosed in a sealed container. A spectrometer (QEpro, Ocean Optics Inc.) with a spectral range of 185-1100 nm and a resolution of 0.14 nm is connected to the other input port for measuring the reflection spectrum. A computer is used to record the reflection spectrum and analyze the wavelength shift caused by the concentration change of VOC gas. Figure 1(b) is the manufacturing process of the fiber optic probe. Figure 1(c) shows the schematic of the CLCF-coated fiber end face. Figure 2(a) shows the relationship between CLCF thickness and reflection spectrum. It can be seen the peak of reflection spectrum rises higher as the thickness increases. In order to select an appropriate CLCF thickness, we measured the relationship between the wavelength shift and the acetone concentration at different thicknesses, and the results are shown in Fig. 2(b). It can be seen from Fig. 2(b) that when the thickness of CLCF is 14 µm or 31 µm, R^2=0.92 or 0.96. When the thickness of CLCF is 40 µm and 63 µm, R^2 = 0.99, but the slope of the fitting curve is higher at 40 µm. Obviously the slope and linearity of fitting curve are the highest at 40 µm in these cases, hence we select a CLCF thickness of

Optics EXPRESS

40 μm to make it more sensitive to acetone gas in our experiment. Since the CLCF is formed by photo-crosslinking, it is not easily peeled from the fiber end. In our experiments, a certain amount of liquid VOC is carefully injected into a 400 mL sealed container with a syringe and quickly evaporated in the container. Therefore, the concentration of VOC gas in the container can be calculated. The experiments were carried out at room temperature (20°C).

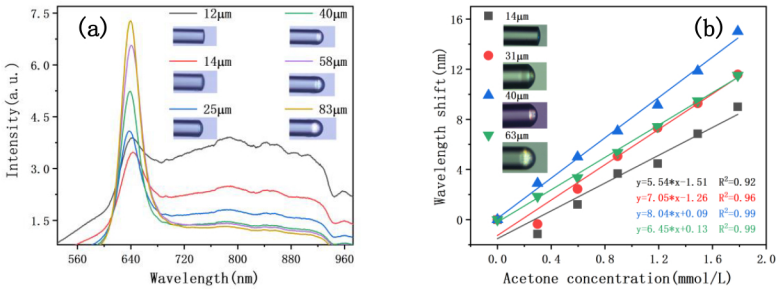

Fig. 2. (a) Reflectance spectrum under different CLCF thickness; (b) the relationship between acetone gas concentration and wavelength shift under different CLCF thicknesses.

3.2. *Sensing characteristics of fiber optic dual-probe sensor for acetone and ethanol gas*

In order to determine the maximum detection range and detection limit of the sensor for acetone gas, we have conducted related experiments and the results are shown in Fig. 3. Figure 3(a) is the reflectance spectrum of No.1 CLCF at different acetone gas concentrations. We gradually added acetone gas in a closed container equipped with sensor probe until the reflection band of CLCF disappeared, and recorded the acetone gas concentration as 15.496 mmol/L (378877 ppm). Then we placed sensor probe in a new airtight container and increased the acetone gas concentration until the reflection spectrum shifted. The result is shown in Fig. 3(b) that the reflection spectrum drifts at a concentration of 0.025 mmol/L (630 ppm) and the center wavelength shifts by 0.54 nm. Therefore, for acetone gas, the maximum detection concentration of the sensor is 15.496 mmol/L (378877 ppm), and the detection limit is 0.025 mmol/L (630 ppm).

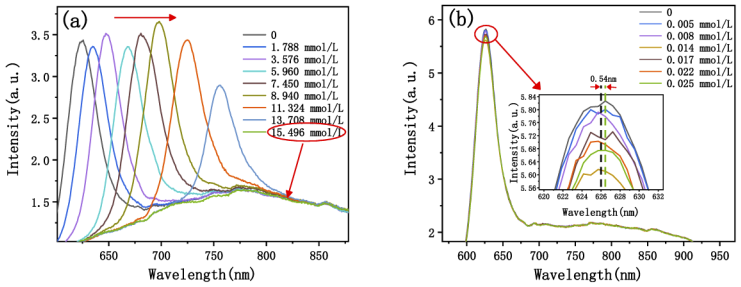

Fig. 3. Reflectance spectra of No.1 CLCF at different acetone gas concentrations: (a) detection range; (b) detection limit.

Figures 4(a) and 4(c) show the reflection spectra of the sensor in different concentrations of acetone gas and ethanol gas, respectively. The inserted graph shows the spectrum of the light source. Two reflection peaks corresponding to two CLCFs appear in the spectra, and as the gas concentration increases, the wavelengths of both reflection peaks shift to the red side. Redshift means that VOC gas molecules bond with the CLC molecules and expand the helical pitch of CLC.

Optics EXPRESS

The dependence of the peak wavelength on the acetone gas concentration is described in Fig. 4(b), and linear fits are applied to the experimental data to obtain the sensitivities. The sensitivity of No.1 CLCF is 8.435 nm·L/mmol (3.45×10^{-4} ppm/nm), $R^2 = 0.997$, and the sensitivity of No.2 CLCF is 14.867 nm·L/mmol (6.082×10^{-4} ppm/nm), $R^2 = 0.999$. Among them, nm·L/nmol means the distance that 1 mmol/L gas causes the spectrum to move [23]. The relationship between the peak wavelength and the ethanol gas concentration is exhibited in Fig. 4(d) and the sensitivities of No.1 CLC and No.2 CLC are 14.856 nm·L/mmol (6.082×10^{-4} ppm/nm), $R^2 = 0.894$ and 29.303 nm·L/mmol (1.186×10^{-3} ppm/nm), $R^2 = 0.993$, respectively. The results indicate that No.2 CLC is more sensitive to the change of the gas concentration, which might be related to the short-range attraction of the interaction between organic vapor and No.2 CLC molecules. In addition, these two CLCFs are more sensitive to ethanol gas than to acetone gas. Although both the acetone gas and ethanol gas are composed of polar molecules, the polarity of ethanol molecules is larger than that of acetone molecules. As a result, CLC molecules can interact with ethanol molecules more effectively and present a higher sensitivity to ethanol gas [33].

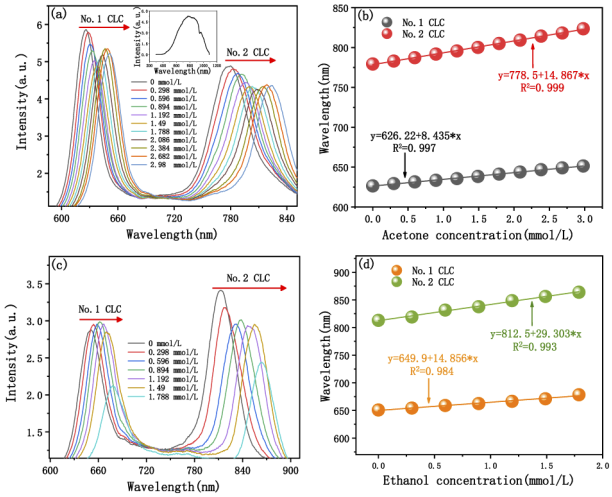

Fig. 4. In acetone gas environment: (a) reflection spectra (b) sensitivities; In ethanol gas environment: (c) reflection spectra (d) sensitivities.

To investigate the repeatability of the sensor, we repeatedly measure the spectral response three times at the acetone concentration of 0 - 2.98 mmol/L, which are shown in Fig. 5. The sensitivities of No.1 CLCF are 8.117 nm·L/mmol, 8.432 nm·L/mmol and 8.404 nm·L/mmol, and the sensitivities of No.2 CLCF are 13.244 nm·L/mmol, 14.711 nm·L/mmol and 14.627 nm·L/mmol. For No.1 CLC, the deviations of these three fitted lines are small, and the maximum relative deviation of the sensitivity is less than 3.7%, which indicates that No.1 CLCF has excellent repeatability. For No.2 CLCF, the maximum relative deviation of the sensitivity is 10%, which might be caused by the higher sensitivity of No.2 CLCF to the gas. However, the deviation of each fitted line is still small, and we consider that No.2 CLCF has good repeatability.

In order to study the dynamic response of the sensor, multiple measurements between 0 and 0.8 mmol/L are repeated. In the experiment, fiber probes are first inserted into the first sealed container without the acetone gas, and the spectrometer records the peak wavelengths of the reflection spectrum. We draw 0.023 mL acetone liquid into the syringe in advance. After the acetone liquid is fully evaporated into gas in the syringe, it is rapidly injected into the container. As a result, the concentration of acetone gas in the container will increase from 0 to 0.8 mmol/L. The spectrometer continuously monitors the shifts of the peak wavelengths. When the reflection

Optics EXPRESS

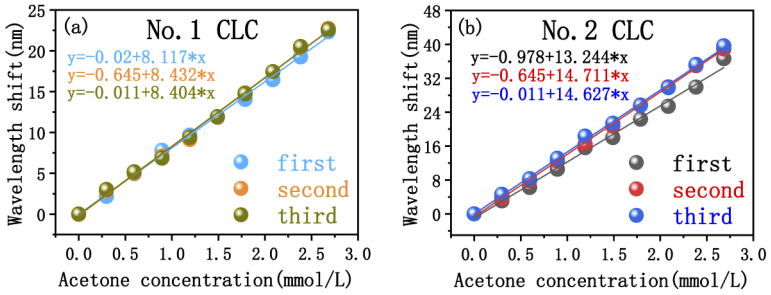

Fig. 5. Repeatability test of the sensor: (a) Three times of measurements of No.1 CLCF and (b) three times of measurements of No.2 CLCF.

spectrum is stable for a while, we quickly put the fiber optic probe into the air. Repeat the measurement three times, the dynamic responses of No.1 CLCF and No.2 CLCF are shown in Fig. 6. It can be seen that the three cycles have the same variation in the wavelength shift, which indicates the CLCF has good reversibility and repeatability.

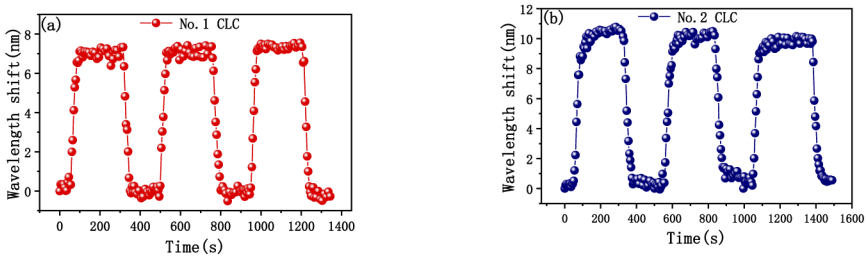

Fig. 6. Dynamic responses of the fiber probes for repeated exposures to 0.8 mmol/L of acetone (a) No.1 CLCF; (b) No.2 CLCF.

Figures 7(a) and 7(b) shows a cycle of the variation in the wavelength shifting of the two CLCFs. It can be seen from the figure that the response time of No.1 CLCF and No.2 CLCF are 45s and 70s, respectively, and the recovery process requires are 45s and 65s. By comparing the two sets of data, it can be seen that the response time and recovery time of No.1 CLCF are faster. This is due to the lower sensitivity of No. 1 CLCF and less acetone gas absorption, so the response time and recovery time are faster than No.2 CLCF. In order to verify the repeatability of the two CLCFs, multiple measurements between 0 and 1.4 mmol/L are repeated. Figures 7(c) and 7(d) show the spectral responses of seven repeated measurements. For No.1 CLC peak wavelength, the maximum deviation in the air is 0.26 nm, the relative standard deviation in the air is 0.049%, the maximum deviation in 0.745 mmol/L is 0.68 nm, and the relative standard deviation in 1.4 mmol/L is 0.051%. For No.2 CLC peak wavelength, the maximum deviation in the air is 0.62 nm, the relative standard deviation in the air is 0.049%, the maximum deviation in 1.4 mmol/L is 0.68 nm, and the relative standard deviation in 1.4 mmol/L is 0.062%. These results further verify that the sensor has good repeatability.

To investigate the effect of humidity on the sensor, we measured the relationship between the humidity and the peak wavelength of the CLC. The sensor probe was placed into the temperature and humidity chamber. The temperature in the chamber was fixed at 25°C and the relative humidity was set to increase from 49% to 82%. Since the two CLCFs have the same composition, we tested No.2 CLCF. As shown by the scatters in Figs. 8(a) and 8(b), the wavelength shifts 0.9 nm in the humidity range of 49%–82%. The influence of the relative humidity on the sensor

Optics EXPRESS

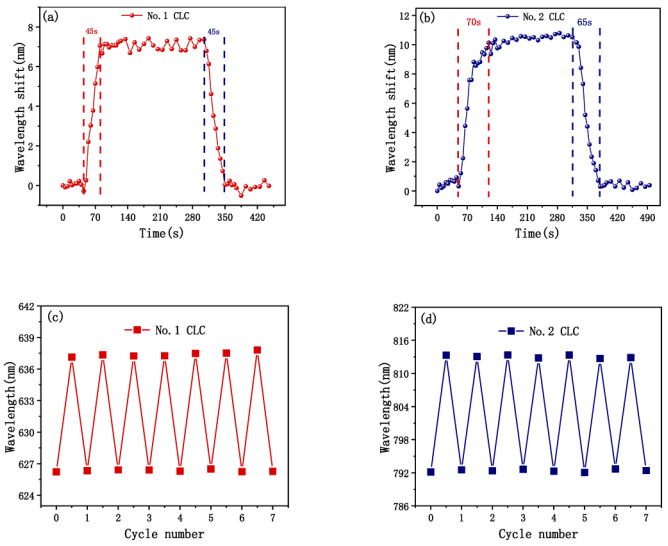

Fig. 7. Dynamic responses at the acetone gas concentration of 0-0.8 mmol/L: (a) No.1 CLCF and (b) No.2 CLCF. Spectral responses of seven repeated measurements of the peak wavelength at the acetone gas concentrations of 0 and 0.1.4 mmol/L: (c) No.1 CLCF and (d) No.2 CLCF.

can be ignored in sensing the concentration of the VOC-gas since the fluctuation of the relative humidity in the chamber is less than 1.5%.

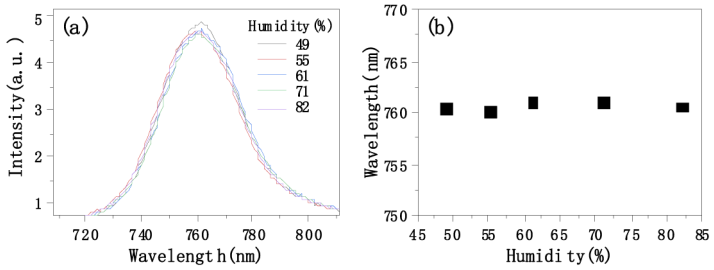

Fig. 8. Dependence of peak wavelength of No.2 CLC on relative humidity at 25°C: (a) reflection spectra and (b) peak wavelength scatter plot.

We investigate the effects of mixing ratio of acetone and ethanol gases and the total gas concentration on wavelength shift. Figure 9 shows the dependence of the wavelength shift on the total concentration of the mixed gas at different mixing ratios of acetone to ethanol, in which both CLCFs present higher sensitivities to the mixed gas with a higher ethanol concentration. This phenomenon can be explained by the strong polarity of the ethanol molecules, which results in the mixed gas with a high concentration of ethanol gas having a strong total polarity. Therefore, at the same total concentration, the higher the ethanol content, the larger the wavelength shift.

Figure 9 shows that both the total gas concentration and the mixing ratio of acetone to ethanol influence the wavelength shift $\Delta\lambda$ of CLC. Therefore, the linear relationship between $\Delta\lambda$, the total gas concentration and the mixing ratio of acetone to ethanol can be expressed as:

$$\Delta\lambda = AX + BY \tag{1}$$

Optics EXPRESS

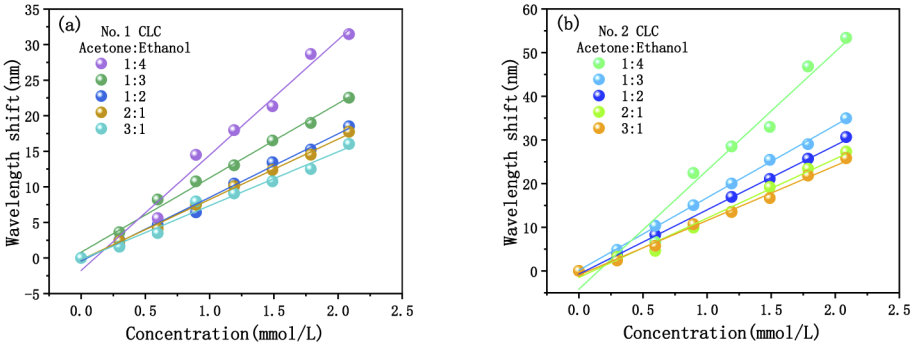

Fig. 9. Dependence of the CLC wavelength shift on the total concentration of the mixed gas at different mixing ratios of acetone to ethanol: (a) No.1 CLCF and (b) No.2 CLCF.

where A and B are sensing coefficients, X is the total gas concentration, and Y is the ratio of acetone to ethanol. When the total concentration is constant, an increase in the proportion of ethanol gas will result in an increase in $\Delta\lambda$, whereas an increase in the proportion of acetone gas will cause a decrease in $\Delta\lambda$. Therefore, B is negative. However, the concentrations of acetone and ethanol cannot be obtained by a single relational expression. Our dual-probe design can definitely solve this problem. The relationship matrix can be written as fellows:

$$\begin{bmatrix} \Delta\lambda_1 \\ \Delta\lambda_2 \end{bmatrix} = \begin{bmatrix} A_1 & B_1 \\ A_2 & B_2 \end{bmatrix} \begin{bmatrix} X \\ Y \end{bmatrix} \tag{2}$$

where $\Delta\lambda_1$ and $\Delta\lambda_2$ are peak shifts of No.1 CLCF and No.2 CLCF, respectively, A_1 and B_1 are sensing coefficients of No.1 CLCF, and A_2 and B_2 are sensing coefficients of No.2 CLCF. Figure 10 shows contour plots of $\Delta\lambda$ as a function of the total gas concentration and acetone/ethanol ratio.

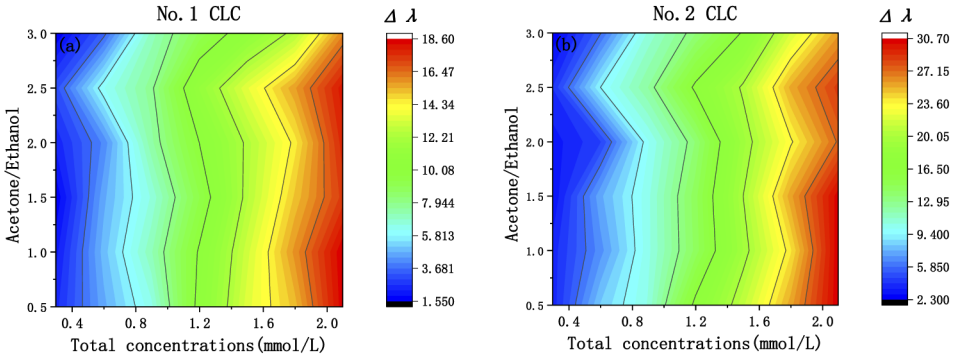

Fig. 10. Contour plots of $\Delta\lambda$ versus gas concentration and ratio of acetone to ethanol: (a) No.1 CLCF and (b) No.2 CLCF.

Based on the experimental results, a least-squares method is adopted to determine A and B in Eq. (2), which is shown in Table 1. It can be seen that A_2 is larger than A_1, which indicates that No. 2 CLCF is more sensitive. This result is consistent with the results of previous measurements. The gas concentration and the ratio of acetone to ethanol can be determined by applying Eq. (2).

Optics EXPRESS

Table 1. Determined sensing coefficients by the least-squares method.

	No.1 CLCF	No.2 CLCF
A	8.57	14.36
B	−0.19	−0.97

4. Conclusions

In conclusion, a dual-probe fiber optic sensor for detecting VOC gas is fabricated by coating two CLCFs with different reflection wavelengths on the two fiber end faces of a 2×2 multimode fiber coupler. The sensitivities of CLCFs to acetone and ethanol are obtained by monitoring the peak wavelength shifts at different gas concentrations. The experimental results show that the sensitivities of the two CLCFs are 8.435 nm·L/mmol (3.45×10^{-4} ppm/nm) and 14.867 nm·L/mmol (6.082×10^{-4} ppm/nm) to acetone gas, 14.856 nm·L/mmol (6.082×10^{-4} ppm/nm) and 29.303 nm·L/mmol (1.186×10^{-3} ppm/nm) to ethanol gas. They all present good linearity, stability and repeatability. In addition, according to the different sensitive responses of CLCFs to acetone gas and alcohol gas, the linear relationship between $\Delta\lambda$, total mixed gas concentration and acetone/ ethanol ratio can also be obtained from the experimental results using the least-squares method. Therefore, this dual-probe fiber optic sensor can distinguish the concentrations of two VOC gases in their mixture.

Funding

National Natural Science Foundation of China (U1531102, 61107059); Lanzhou Institute of Physics (ZWK1801); National Natural Science Foundation of Heilongjiang (A2018002).

Disclosures

The authors declare no conflicts of interest.

References

1. B. F. Yu, Z. B. Hu, M. Liu, H. L. Yang, Q. X. Kong, and Y. H. Liu, "Review of research on air-conditioning systems and indoor air quality control for human health," Int. J. Refrig. **32**(1), 3–20 (2009).
2. R. Malik, V. K. Tomer, T. Dankwort, Y. K. Mishra, and L. Kienle, "Cubic mesoporous Pd–WO_3 loaded graphitic carbon nitride (g-CN) nanohybrids: highly sensitive and temperature dependent VOC sensors," J. Mater. Chem. A **6**(23), 10718–10730 (2018).
3. T. Saidi, O. Zaim, M. Moufid, N. El Bari, R. Ionescu, and B. Bouchikhi, "Exhaled breath analysis using electronic nose and gas chromatography–mass spectrometry for non-invasive diagnosis of chronic kidney disease, diabetes mellitus and healthy subjects," Sens. Actuators, B **257**, 178–188 (2018).
4. A. Mirzaei, J. H. Kim, H. W. Kim, and S. S. Kim, "Resistive-based gas sensors for detection of benzene, toluene and xylene (BTX) gases: a review," J. Mater. Chem. C **6**(16), 4342–4370 (2018).
5. M. Fernandez-Vallejo and M. Lopez-Amo, "Optical fiber networks for remote fiber optic sensors," Sensors **12**(4), 3929–3951 (2012).
6. H. E. Joe, H. Yun, S. H. Jo, M. B. G. Jun, and B. K. Min, "A Review on Optical Fiber Sensors for Environmental Monitoring," Int. J. of Precis. Eng. and Manuf.-Green Tech. **5**(1), 173–191 (2018).
7. W. U. Bin-Qing, C. L. Zhao, and Z. M. Ding, "Sagnac Interferometer Fiber Volatile Organic Compounds Sensor Based on PDMS," Acta Photonica Sinica **46**(1), 106003 (2017).
8. A. Cao, R. J. H. V. Raak, X. Pan, and D. J. Broer, "Temperature- and Light-Regulated Gas Transport in a Liquid Crystal Polymer Network," Adv. Funct. Mater. **29**(28), 1900857 (2019).
9. Y. V. Kaneti, J. Moriceau, M. Liu, Y. Yuan, Q. Zakaria, X. Jiang, and A. Yu, "Hydrothermal synthesis of ternary α-Fe_2O_3–ZnO–Au nanocomposites with high gas-sensing performance," Sens. Actuators, B **209**, 889–897 (2015).
10. Y. H. Li, C. Z. Cai, Y. H. Gu, W. D. Cheng, W. Xiong, and C. J. Zhao, "Novel electronic properties of a new MoS_2/TiO_2 heterostructure and potential applications in solar cells and photocatalysis," Appl. Surf. Sci. **414**, 34–40 (2017).
11. K. M. Tripathi, T. Kim, D. Losic, and T. T. Tung, "Recent advances in engineered graphene and composites for detection of volatile organic compounds (VOCs) and non-invasive diseases diagnosis," Carbon **110**, 97–129 (2016).

Optics EXPRESS

12. X. P. Ning, C. L. Zhao, J. Y. Yang, and C. C. Chan, "Zeolite thin film-coated spherical end-face fiber sensors for detection of trace organic vapors," Opt. Commun. **364**, 55–59 (2016).
13. M. Pacquiao, M. D. De Luna, N. Thongsai, S. Kladsomboon, and P. Paoprasert, "Highly fluorescent carbon dots from enokitake mushroom as multi-faceted optical nanomaterials for Cr^{6+} and VOC detection and imaging applications," Appl. Surf. Sci. **453**, 192–203 (2018).
14. Z. Xiong, C. Zhang, J. Hu, D. Fu, Y. Lu, W. Sun, and Y. Liu, "Thermal and electrical tuning of whispering gallery modes in liquid crystal-filled hollow glass microsphere," Appl. Phys. Express **12**(2), 022003 (2019).
15. D. H. Yeo and S. Y. Park, "Liquid-crystal-based biosensor for detecting Ca^{2+} in human saliva," J. Ind. Eng. Chem. (Amsterdam, Neth.) **74**, 193–198 (2019).
16. Y. Wang, L. Zhao, A. Xu, L. Wang, L. Zhang, S. Liu, Y. Liu, and H. Li, "Detecting enzymatic reactions in penicillinase via liquid crystal microdroplet-based pH sensor," Sens. Actuators, B **258**, 1090–1098 (2018).
17. Y. Lu, Y. Yang, Y. Wang, L. Wang, J. Ma, L. Zhang, W. Sun, and Y. Liu, "Tunable liquid-crystal microshell-laser based on whispering-gallery modes and photonic band-gap mode lasing," Opt. Express **26**(3), 3277–3285 (2018).
18. K. P. Yang Han, C. W. M. Bastiaansen, D. J. Broer, and R. P. Sijbesma, "Optical Monitoring of Gases with Cholesteric Liquid Crystals," J. Am. Chem. Soc. **132**(9), 2961–2967 (2010).
19. M. Mitov, "Cholesteric liquid crystals with a broad light reflection band," Adv. Mater. **24**(47), 6260–6276 (2012).
20. A. Mujahid, H. Stathopulos, P. A. Lieberzeit, and F. L. Dickert, "Solvent Vapour Detection with Cholesteric Liquid Crystals—Optical and Mass-Sensitive Evaluation of the Sensor Mechanism," Sensors **10**(5), 4887–4897 (2010).
21. C. K. Chang, C. W. M. Bastiaansen, D. J. Broer, and H. L. Kuo, "Discrimination of Alcohol Molecules Using Hydrogen-Bridged Cholesteric Polymer Networks," Macromolecules **45**(11), 4550–4555 (2012).
22. L. Sutarlie, J. Y. Lim, and K. L. Yang, "Cholesteric liquid crystals doped with dodecylamine for detecting aldehyde vapors," Anal. Chem. **83**(13), 5253–5258 (2011).
23. J. Y. Tang, J. B. Fang, Y. L. Liang, B. Zhang, Y. H. Luo, X. Y. Liu, Z. B. Li, X. J. Cai, J. Q. Xian, H. Lin, W. G. Zhu, H. Y. Guan, H. H. Lu, J. Zhang, J. H. Yu, and Z. Chen, "All-fiber-optic VOC gas sensor based on side-polished fiber wavelength selectively coupled with cholesteric liquid crystal film," Sens. Actuators, B **273**, 1816–1826 (2018).
24. M. Bedolla-Pantoja and N. L. Abbott, "Surface-Controlled Orientational Transitions in Elastically Strained Films of Liquid Crystal That Are Triggered by Vapors of Toluene," ACS Appl. Mater. Interfaces **8**(20), 13114–13122 (2016).
25. C. K. Chang, H. L. Kuo, K. T. Tang, and S. W. Chiu, "Optical detection of organic vapors using cholesteric liquid crystals," Appl. Phys. Lett. **99**(7), 073504 (2011).
26. K. J. Kek, J. J. Z. Lee, Y. Otono, and S. Ishihara, "Chemical gas sensors using chiral nematic liquid crystals and its applications," J. Soc. Inf. Disp. **25**(6), 366–373 (2017).
27. N. Kirchner, L. Zedler, T. G. Mayerhofer, and G. J. Mohr, "Functional liquid crystal films selectively recognize amine vapours and simultaneously change their colour," Chem. Commun. **14**, 1512–1514 (2006).
28. P. V. Shibaev, D. Carrozzi, L. Vigilia, and H. DeWeese, "Liquid crystal nose, chiral case: towards increased selectivity and low detection limits," Liq. Cryst. **46**(9), 1309–1317 (2019).
29. L. Sutarlie, H. Qin, and K. L. Yang, "Polymer stabilized cholesteric liquid crystal arrays for detecting vaporous amines," Analyst **135**(7), 1691–1696 (2010).
30. P. V. Shibaev, M. Wenzlick, J. Murray, A. Tantillo, and J. Howard-Jennings, "Liquid Crystalline Compositions as Gas Sensors," Mol. Cryst. Liq. Cryst. **611**(1), 94–99 (2015).
31. O. Aksimentyeva, Z. Mykytyuk, A. Fechan, O. Sushynskyy, and B. Tsizh, "Cholesteric Liquid Crystal Doped by Nanosize Magnetite as an Active Medium of Optical Gas Sensor," Mol. Cryst. Liq. Cryst. **589**(1), 83–89 (2014).
32. C. K. Chang, S. W. Chiu, H. L. Kuo, and K. T. Tang, "Cholesteric liquid crystal-carbon nanotube hybrid architectures for gas detection," Appl. Phys. Lett. **100**(4), 043501 (2012).
33. A. Joshi, V. Manjuladevi, R. K. Gupta, and S. Kumar, "Morphological transformation in the supramolecular assembly of discotic liquid crystal molecules using silver nanoparticles and its sensing application," Nanotechnology **31**(36), 365605 (2020).